Electron energy losses and cathodoluminescence from complex plasmonic nanostructures: spectra, maps and radiation patterns from a generalized field propagator

Arnaud Arbouet, Adnen Mlayah, Christian Girard, Gérard Colas Des Francs

New Journal of Physics
The open access journal at the forefront of physics

Deutsche Physikalische Gesellschaft DPG IOP Institute of Physics

PAPER • OPEN ACCESS

Electron energy losses and cathodoluminescence from complex plasmonic nanostructures: spectra, maps and radiation patterns from a generalized field propagator

To cite this article: Arnaud Arbouet *et al* 2014 *New J. Phys.* **16** 113012

New Journal of Physics
The open access journal at the forefront of physics
Deutsche Physikalische Gesellschaft DPG | IOP Institute of Physics

Electron energy losses and cathodoluminescence from complex plasmonic nanostructures: spectra, maps and radiation patterns from a generalized field propagator

Arnaud Arbouet[1], Adnen Mlayah[1], Christian Girard[1] and Gérard Colas des Francs[2]

[1] CEMES, CNRS and Université de Toulouse, 29, rue Jeanne Marvig 31055 Toulouse Cedex 4, France
[2] Laboratoire Interdisciplinaire Carnot de Bourgogne (ICB), UMR 6303 CNRS, Université de Bourgogne, 9 Avenue Savary, BP 47870, 21078 Dijon Cedex, France
E-mail: arbouet@cemes.fr

Received 13 June 2014, revised 17 August 2014
Accepted for publication 18 September 2014
Published 4 November 2014
New Journal of Physics **16** (2014) 113012
doi:10.1088/1367-2630/16/11/113012

Abstract

We present a unified framework for the description of the interaction of fast electrons with complex nanostructures based on the Green dyadic method. We show that the computation of a generalized field propagator yields the electron energy losses and cathodoluminescence of nano-objects of arbitrary morphologies embedded in complex dielectric media. Spectra and maps for both penetrating and non-penetrating electron trajectories are provided. This numerical approach can be extended to describe complex experiments involving fast electrons and optically excited nanostructures.

Keywords: electron energy loss spectroscopy, cathodoluminescence, plasmonics, nano-optics, EELS, surface plasmons, transmission electron microscopy

1. Introduction

Energy losses from fast electrons have provided the first experimental evidence of surface plasmons (SP) in metallic films (Powell and Swan 1959) and nano-objects (Fujimoto *et al* 1967). Stimulated by both instrumental (monochromators, detectors) and methodological (signal deconvolution and processing) advances, electron energy loss spectroscopy (EELS) and cathodoluminescence (CL) have since demonstrated their unique potential in probing SPs of metallic nanostructures with nanometer spatial resolution (García de Abajo and Kociak 2008a, Sigle *et al* 2009, García de Abajo 2010, García de Abajo and Kociak 2008b, Alber *et al* 2012, Carbone *et al* 2009, Sigle *et al* 2009, Geuquet and Henrard 2010, Howie 2009, Myroshnychenko *et al* 2012, Scholl *et al* 2012, Bosman *et al* 2013). Besides the superior spatial resolution compared to optical techniques, the ability of fast electrons to probe the dark SP modes and provide simultaneously accurate information on the morphology and environment of the investigated nano-objects has given a central role to electron spectroscopies in experimental nanoplasmonics. Today, these techniques are used to investigate nanostructures of increasing complexity in which the particle morphology, the substrate or the interparticle interactions strongly influence their optical response. In return, the interpretation of these sophisticated experiments has stimulated the development of several simulation techniques based on the boundary element method (BEM) (García de Abajo *et al* 2002, Hohenester and Trügler 2012) or discrete dipole approximation (DDA) (Geuquet and Henrard 2010), for instance. The connection of the electron energy loss probability with the local density of electromagnetic modes of metallic particles has been analyzed in detail (García de Abajo and Kociak 2008a, Hohenester *et al* 2009, Boudarham and Kociak 2012). Recent advances in combined electron/optical spectroscopy techniques such as electron energy gain spectroscopy demonstrated in ultrafast transmission electron microscopes (TEM) or surface plasmon three-dimensional (3D) imaging push forward the need and development of novel simulation techniques (Hohenester *et al* 2009, Nicoletti *et al* 2013, Hörl *et al* 2013, Rivacoba and Zabala 2014, Park and Zewail 2014).

In this article, we extend the 3D Green dyadic method (3D-GDM) and show that several aspects of the interaction of fast electrons with nanostructures, namely electron energy losses and CL can be accurately described using a generalized field propagator. The GDM is a well-established technique and is particularly well-suited for the description of the optical properties of nanostructures of arbitrary geometries, either isolated or electromagnetically coupled to other nano-objects or located in the vicinity of planar interfaces (Girard and Dereux 1996, Tripathy *et al* 2011). Besides the far-field and near-field optical properties, the GDM has been used to predict the temperature increase induced in plasmonic particles by an optical excitation (Baffou *et al* 2010), to describe scanning optical microscopy experiments (Teulle *et al* 2012) or to visualize the 3D charge distribution associated with surface plasmon excitations (Marty *et al* 2010). In this work, we extend the 3D-GDM to more complex scenarios involving fast electrons interacting with plasmonic nanostructures.

As depicted in figure 1, we first present the calculation of the energy losses of a fast electron impinging on a metallic nanostructure located on a substrate. The latter can be a simple homogeneous medium, but more complex cases, such as layered substrates, can also be considered. The electron is travelling along the (OZ) axis with a velocity $\mathbf{v} = -v\ \mathbf{e}_z$ and the substrate surface is the (OXY) plane. The metallic particle with permittivity $\varepsilon_m(\omega)$ is lying on

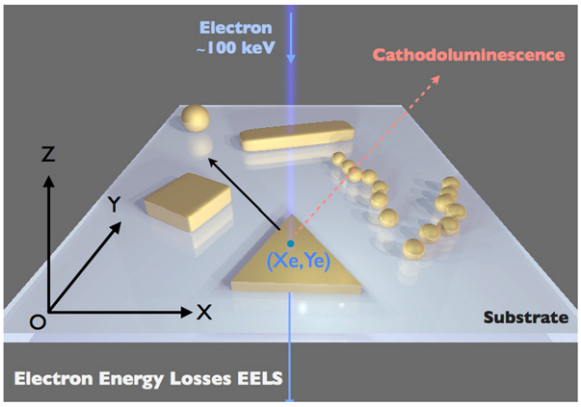

Figure 1. A fast electron incident along the (OZ) axis interacts with metallic nanostructures located on a dielectric substrate. The substrate plane is (OXY). The absolute (XYZ) frame is used to define the electron location.

the substrate of dielectric constant ε_{sub} and is surrounded by a medium of dielectric constant ε_{env}.

The moving electron creates both charge and current distributions that can be written $\rho(\mathbf{r}, t) = -e\,\delta(\mathbf{r} - \mathbf{r}_e(t))$ and $\mathbf{j}(\mathbf{r}, t) = -e\,\delta(\mathbf{r} - \mathbf{r}_e(t))\,\mathbf{v}$, respectively. These two spatio-temporal distributions are the sources of an electric field $\mathbf{E}_{\text{el}}(\mathbf{r}, t)$ that can be derived from Maxwell's equations (Jackson 1998). In the $(\mathbf{r}, \omega)$ space, the Fourier components of $\mathbf{E}_{\text{el}}(\mathbf{r}, t)$ can be written (in CGS units):

$$\mathbf{E}_{\text{el}}(\mathbf{r}, \omega) = -\frac{e\,\omega}{\pi v^2 \gamma \varepsilon_{\text{env}}} \mathrm{e}^{-\frac{\mathrm{i}\,\omega z}{v}} \left[\frac{i}{\gamma} K_0\left(\frac{\omega R}{v\gamma}\right)\mathbf{e}_z + K_1\left(\frac{\omega R}{v\gamma}\right)\mathbf{e}_R \right], \tag{1}$$

where $\gamma = 1/\sqrt{1 - \varepsilon_{\text{env}} v^2/c^2}$ is the Lorentz contraction factor and cylindrical coordinates are used ($\mathbf{r} = R\,\mathbf{e}_R + z\,\mathbf{e}_z$). For a 100 kV incident electron, $v \approx 0.5c$ and $\gamma = 1.2$. K_0 and K_1 are modified Bessel functions of the second kind. Rigorously, equation 1 should be modified to account for the electron interaction with interfaces between two different media. As detailed in the appendix, these corrections can be calculated from the boundary conditions and remain small outside of a thin layer above and below the interface. In the appendix, we show that their influence on the computed energy losses is weak. In the following, we have discarded these corrections to minimize the required computational ressources and used the bulk expression $\mathbf{E}_{\text{el}}(\mathbf{r}, \omega)$ in the EELS and CL simulations. Note that the electric field scattered by the nanostructures is calculated taking into account the substrate (see equations 10 and below). Only the incident field is approximated by its expression for an homogeneous medium (see also appendix). The contribution from Cherenkov radiation is not considered in the following.

2. Electron energy losses from a generalized field propagator

In this section, we show that it is possible to accurately compute the energy losses of a fast electron incident on any nanostructure from a generalized field propagator. The electric field associated with the electron induces a polarization distribution $\mathbf{P}(\mathbf{r}, \omega)$ inside the nanostructures. In turn, $\mathbf{P}(\mathbf{r}, \omega)$ generates a secondary electric field $\mathbf{E}_{\text{ind}}(\mathbf{r}', \omega)$. The work accumulated by the electron against the Lorentz force decreases its kinetic energy by (García de

Abajo 2010):

$$\Delta E_{\mathrm{EELS}} = e \int \mathrm{d}t \ \mathbf{v}.\ \mathbf{E}_{\mathrm{ind}}\big(\mathbf{r}_e(t),\, t\big) \tag{2}$$

$$= \int_0^{+\infty} E \ \mathrm{d}E \ \Gamma_{\mathrm{EELS}}(E), \tag{3}$$

where $\Gamma_{\mathrm{EELS}}(E)$ is the electron energy loss probability per unit energy (García de Abajo 2010):

$$\Gamma_{\mathrm{EELS}}(E) = \frac{2e}{\hbar^2\omega} \int_{-\infty}^{+\infty} \mathrm{d}t \ \mathrm{Re}\Big[\ \mathbf{v}.\ \mathbf{E}_{\mathrm{ind}}\big(\mathbf{r}_e(t),\, E\big)\mathrm{e}^{-\mathrm{i}Et/\hbar}\Big]. \tag{4}$$

In this equation, the Fourier component of the induced electric field $\mathbf{E}_{\mathrm{ind}}(\mathbf{r},\, \omega)$ can be calculated from the Green dyadic tensor $\mathbf{S}(\mathbf{r},\, \mathbf{r}',\, \omega)$ of the environment that connects $\mathbf{E}_{\mathrm{ind}}(\mathbf{r},\, \omega)$ to the polarization distribution $\mathbf{P}(\mathbf{r}',\, \omega)$ (Martin *et al* 1995, Girard 2005):

$$\mathbf{E}_{\mathrm{ind}}(\mathbf{r},\, \omega) = \int_V \mathbf{S}(\mathbf{r},\, \mathbf{r}',\, \omega) \cdot \mathbf{P}(\mathbf{r}',\, \omega)\mathrm{d}\mathbf{r}' \ , \tag{5}$$

where V is the volume of the nanostructure.

Assuming a local response of the metal, the electric susceptibility $\chi(\mathbf{r}',\, \omega)$ can be defined as:

$$\begin{aligned} \chi(\mathbf{r}',\, \omega) &= \frac{\varepsilon_{\mathrm{m}}(\omega) - \varepsilon_{\mathrm{env}}}{4\pi} \quad \text{if } \mathbf{r}' \in V \\ \chi(\mathbf{r}',\, \omega) &= 0 \qquad\qquad\quad \text{elsewhere.} \end{aligned} \tag{6}$$

Then, the Fourier components $\mathbf{E}_{\mathrm{ind}}(\mathbf{r},\, \omega)$ of the induced electric field are:

$$\mathbf{E}_{\mathrm{ind}}(\mathbf{r},\, \omega) = \int_V \mathrm{d}\mathbf{r}'\mathbf{S}(\mathbf{r},\, \mathbf{r}',\, \omega) \cdot \chi(\mathbf{r}',\, \omega) \cdot \mathbf{E}(\mathbf{r}',\, \omega), \tag{7}$$

in which $\mathbf{E}(\mathbf{r}',\, \omega)$ is the self-consistent electric field in the nanostructure. This relation can be recast with a generalized propagator $\mathcal{P}(\mathbf{r},\, \mathbf{r}',\, \omega)$ that directly connects the electric field induced everywhere in the system to the electric field of the probing electron itself:

$$\mathbf{E}_{\mathrm{ind}}(\mathbf{r},\, \omega) = \int_V \mathrm{d}\mathbf{r}'\mathcal{P}(\mathbf{r},\, \mathbf{r}',\, \omega) \cdot \mathbf{E}_{\mathrm{el}}(\mathbf{r}',\, \omega) \tag{8}$$

$\mathcal{P}(\mathbf{r},\, \mathbf{r}',\, \omega)$ is then given by:

$$\mathcal{P}(\mathbf{r},\, \mathbf{r}',\, \omega) = \chi(\mathbf{r}',\, \omega) \cdot \mathcal{S}(\mathbf{r},\, \mathbf{r}',\, \omega), \tag{9}$$

in which the Green dyadic tensor $\mathcal{S}(\mathbf{r},\, \mathbf{r}',\, \omega)$ ensures self-consistency through:

$$\begin{aligned} \mathcal{S}(\mathbf{r},\, \mathbf{r}',\, \omega) = \mathbf{S}(\mathbf{r},\, \mathbf{r}',\, \omega) \\ + \int_{\mathrm{V}} \mathrm{d}\mathbf{r}''\mathbf{S}(\mathbf{r},\, \mathbf{r}'',\, \omega) \cdot \chi(\mathbf{r}'',\, \omega) \cdot \mathcal{S}(\mathbf{r}'',\, \mathbf{r}',\, \omega) \end{aligned} \tag{10}$$

This Dyson equation can be solved by applying the numerical method described in (Martin *et al* 1995) for electromagnetic scattering phenomena. The propagator $\mathbf{S}(\mathbf{r},\, \mathbf{r}'',\, \omega)$ is the sum of the vacuum propagator $\mathbf{S}_0(\mathbf{r},\, \mathbf{r}'',\, \omega)$ and the surface propagator $\mathbf{S}_{\mathrm{surf}}(\mathbf{r},\, \mathbf{r}'',\, \omega)$. For the latter, several options are available depending on the investigated situation (type of substrate, influence of retardation effects). In the most simple case, the non-retarded image dipole approximation yields a simple analytical expression of $\mathbf{S}_{\mathrm{surf}}(\mathbf{r},\, \mathbf{r}'',\, \omega)$.

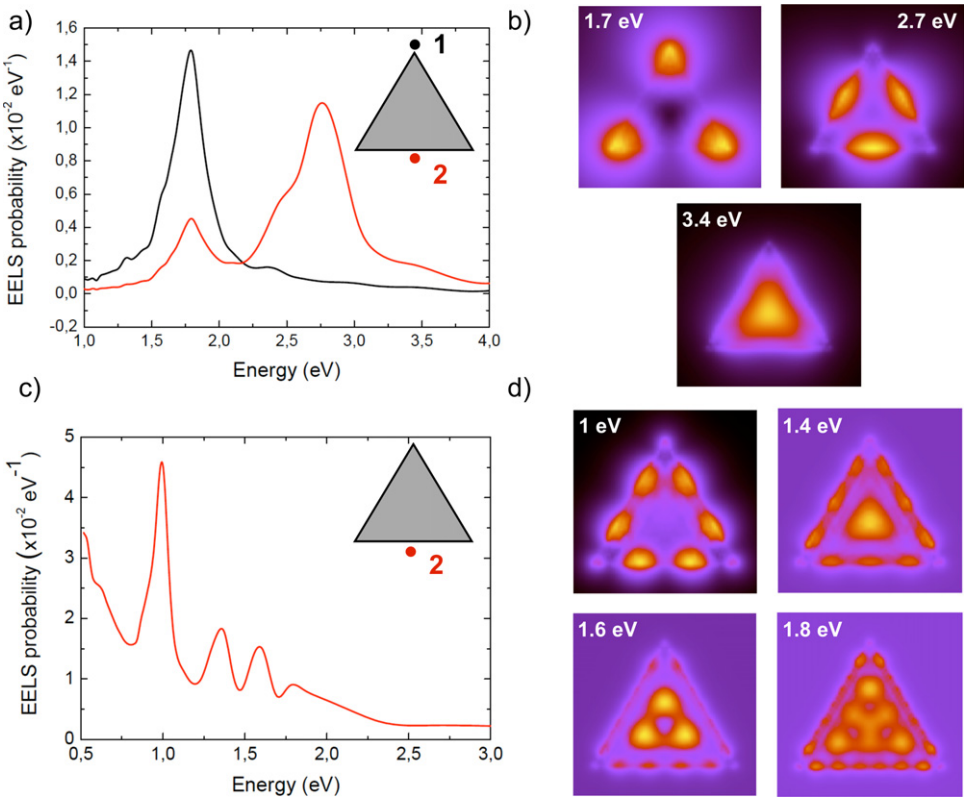

Figure 2. (a) EELS spectra computed for a 100 kV electron incident at 6 nm from the apex (position 1) or middle of an edge (position 2) of a silver nanoprism (edge length $a = 78$ nm, thickness $t = 10$ nm) lying on a mica substrate ($\varepsilon_{sub} = 2.3$). (b) EELS maps computed at 1.7, 2.7 and 3.4 eV. (c) EELS spectra computed at 9 nm from a gold nanoprism edge (edge length $a = 950$ nm, thickness $t = 15$ nm lying on a Si_3N_4 substrate ($\varepsilon_{sub} = 3.9$). The electron kinetic energy is 200 keV. (d) EELS maps computed at 1, 1.4, 1.6 and 1.8 eV. The EELS probability is per electron and per unit energy.

We first illustrate our method by considering a silver nanoprism located on a mica substrate as in (Nelayah *et al* 2007). In figure 2(a), we have computed the EELS of a 100 kV electron, 6 nm away from the apex of a gold nanoprism (position 1) or from the middle of an edge (position 2). The electron energy loss spectra display two clear features at 1.7 and 2.7 eV and a weaker shoulder around 3.4 eV. In figure 2(b), we have generated the EELS maps at these three energies. To do so, the position of the electron beam (X^{elec}, Y^{elec}) is raster scanned over the nanoparticle, and the loss probability $\Gamma_{EELS}(E_{loss})$ is computed at each position for a fixed energy E_{loss}. The computed maps show that the enhanced electron energy losses at 2.7 and 1.7 eV are due to the excitation of quadrupolar and dipolar SP modes, respectively. These three features have been detected and ascribed to different surface plasmon modes (Nelayah *et al* 2007). The excellent agreement with these experiments shows that our method can accurately reproduce both spectra and spatial distributions recorded in EELS experiments (Nelayah *et al* 2007).

As a second example, we now consider the interaction of fast electrons with a larger nanoprism. The gold nanoprism has an edge length of 950 nm and is located on a Si_3N_4 substrate (figure 2(c)). Similar nano-objects have been investigated by EELS, energy-filtered transmission electron microscopy (EFTEM) (Gu *et al* 2011), two-photon photoluminescence (Viarbitskaya *et al*

2013) and dark-field microscopy (Major *et al* 2013). The EELS spectrum is more complex and displays several features at 1, 1.4, 1.6 and 1.8 eV. We have mapped the electron energy loss probability at these four energies (figure 2(d)). The EELS maps, in qualitative agreement with the experimental results of (Gu *et al* 2011), confirm that the obtained features are due to high order SP modes. The latter are similar to the Fabry–Pérot optical cavity modes. With increasing energy, higher order plasmon modes are excited in the metallic resonator, and more nodes are visible. It is worth emphasizing that the inner structure of these modes has not been observed in the experiments most likely because of the large thickness of the investigated nano-objects, which strongly decreases the electron transmission (Gu *et al* 2011).

3. Cathodoluminescence emission probability and radiation pattern from a generalized field propagator

In this part, we show that using the same generalized propagator $\mathcal{P}(\mathbf{r}, \mathbf{r}', \omega)$ of equation 9, another aspect of the interaction of fast electrons with nanostructures, namely, cathodoluminescence (CL), can be quantitatively reproduced. CL is widely used for the nanoscale exploration of the optical properties of semiconductor and metallic nanostructures (Zagonel *et al* 2010). It has recently been extended to measure in a scanning transmission electron microscope (STEM) the second order photon correlation of individual emitting centers in nanodiamonds (Tizei and Kociak 2013). The energy lost by an electron interacting with a metallic nanoparticle is either absorbed (and eventually converted into heat) or re-radiated in the far-field. In metallic nanostructures, the non-radiative inelastic decay channels are much faster than the radiative ones, and therefore light emission is dominated by electron-induced radiation emission; incoherent CL being much weaker (García de Abajo 2010). The coherent CL emission arises from the far-field radiation of the dipoles induced by the evanescent electric field associated with the moving charge. The total radiated energy ΔE_{CL} can be computed from the flux of the Poynting vector (Myroshnychenko *et al* 2012):

$$\Delta E_{CL} = \frac{c}{4\pi} \int \mathrm{d}t \int r^2 d\Omega \; \mathbf{e}_r(\mathbf{E}(\mathbf{r}, t) \wedge \mathbf{H}(\mathbf{r}, t)) \tag{11}$$

$$= \int_0^{+\infty} \hbar\omega \; \mathrm{d}\hbar\omega \int_\Omega \Gamma_{CL}(\Omega, \omega) \; r^2 \mathrm{d}\Omega. \tag{12}$$

The number of photons emitted per electron, unit solid angle and unit energy $\Gamma_{CL}(\Omega, \omega)$ is given by:

$$\Gamma_{CL}(\Omega, \omega) = \frac{1}{\hbar^2 k} \left| \mathbf{E}_{\mathrm{rad}}(\mathbf{r}, \omega) \right|^2. \tag{13}$$

In the latter expression, $\mathbf{E}_{\mathrm{rad}}(\mathbf{r}, \omega)$ is the Fourier transform of the total electric field radiated by the metallic nanostructure and k is the light wavevector in vacuum. $\mathbf{E}_{\mathrm{rad}}(\mathbf{r}, \omega)$ can be computed from the polarization $\mathbf{P}(\mathbf{r}', \omega)$ using the far-field asymptotic expression of the propagator $\mathbf{S}^{\infty}(\mathbf{r}, \mathbf{r}', \omega)$ (Novotny 1997):

$$\mathbf{E}_{\mathrm{rad}}(\mathbf{r}, \omega) = \int_V \mathbf{S}^{\infty}(\mathbf{r}, \mathbf{r}', \omega) \cdot \mathbf{P}(\mathbf{r}', \omega) \mathrm{d}\mathbf{r}' \tag{14}$$

The polarization distribution is obtained from the induced electric field using equations (1) and (8) and the susceptibility (6).

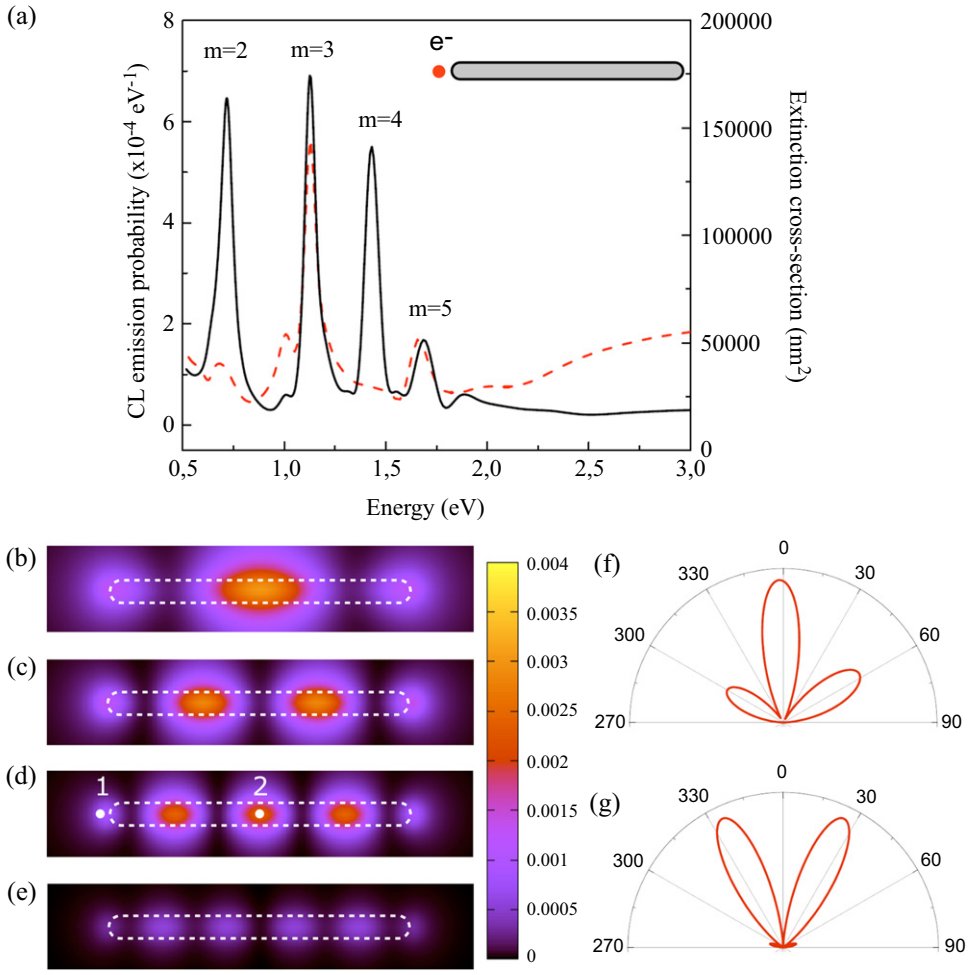

Figure 3. CL photon emission spectrum excited by a 200 kV electron incident on a gold nanowire (length L = 700 nm, diameter D = 50 nm) lying on a substrate with ε_{sub} = 4 (solid line). The dashed line shows the extinction cross-section. The CL emission is collected by a mirror of numerical aperture NA = 0.8. The CL photon emission intensity is given per electron and per unit energy. (b–e) CL photon emission probability maps computed at 0.72, 1.12, 1.42 and 1.69 eV. (f) CL radiation pattern computed at 1.42 eV in a plane containing the nanowire for an electron incident at position 1 (see (d) map). (g) Same at position 2 (see (d) map).

Figure 3(a) shows the CL spectrum collected using a mirror (NA = 0.8) placed above a gold nanowire located on a glass substrate. The electron probe passes 10 nm away from the nanowire end. Our calculations take into account the contribution from the glass substrate and the numerical aperture of the collecting mirror. Four features are clearly visible in figure 3(a) at 0.72, 1.12, 1.42 and 1.69 eV. To shed light on their origin, we have plotted the CL photon emission intensity as a function of the electron beam position at each resonance energy. Figures 3(b)–(e) shows that the spatial distribution of the CL emission probability has a standing wave profile similar to Fabry–Pérot cavity modes. These modes are the counterpart of the high order multipolar surface plasmon modes, evidenced on the EELS maps of figure 2(d). They have already been observed in silver and gold nanowires (Vesseur *et al* 2007, Gómez-

Medina *et al* 2008, Kuttge *et al* 2009) and gold ridges (Coenen *et al* 2012). In our case, the SP resonances at 0.72, 1.12, 1.42 and 1.69 eV are ascribed respectively to the m = 2, 3, 4 and m = 5 surface plasmon resonances of the gold nanowire. A clear advantage of CL spectroscopy, besides its superior spatial resolution, is evidenced in figure 3(a) in which the extinction spectrum of the same nano-object is presented. Unless an asymmetric excitation (e.g. tilted beams) is used, optical spectroscopy techniques relying on plane-wave excitation are restricted to odd–order resonances (Dorfmüller *et al* 2010). Figure 3(a) clearly shows that the $m = 2$ and $m = 4$ resonances are not visible in the optical spectrum. The ability of CL spectroscopy to probe odd and even resonances is a consequence of the strong electric field gradients associated with fast electrons. Furthermore, it has recently been shown that surface plasmon modes of even parity give rise to symmetric Lorentzian lineshapes, whereas modes of odd parity display asymmetric line profiles in the optical extinction spectrum of gold nanorods under near-normal plane-wave illumination (Verellen *et al* 2014). The results of figure 3(a) suggest that this effect also occurs in CL experiments.

Interestingly, relation (13) gives access to the angular distribution of the emitted CL which is another signature of the excited resonances. To illustrate this point we have calculated the angular distribution of the CL from the gold nanowire excited by an electron beam focused either near the end of the nanowire (position 1, figure 3(f)) or at its center (position 2, figure 3(g)) and at the energy of the $m = 4$ resonance. The radiation patterns presented in figures 3(f)–(g) are the result of the interferences of the radiation emitted by the polarization distribution generated in the nano-object. For instance, figure 3(f) shows an asymmetric pattern because the electron excitation is shifted with respect to the center of the nanowire. Figure 3(g) bears close ressemblance with the radiation pattern reported for gold ridges and for the same $m = 4$ resonance using angle-resolved cathodoluminescence experiments (Coenen *et al* 2012).

4. Electron energy losses from nanostructures of arbitrary geometries in the presence of a substrate

The proposed method can also be applied to even more complex morphologies. To further illustrate this, we consider a randomly generated nanostructure consisting of 29 gold nanospheres (diameter $D = 9$ nm) partially or almost completely overlapping and located on a glass substrate (figure 4(a)). Such a morphology mimicks the nanoporous metallic films recently investigated by combined STEM-EELS and high-angle annular dark-field microscopy (HAADF) (Bosman *et al* 2011, Losquin *et al* 2013). The latter studies have demonstrated that the peculiar optical properties of nanoporous metallic films originate from nanoscale variations of the number and spectral properties of the surface plasmon resonances supported by these complex objects with no clear correlation with their local morphology. Figures 4(b)–(d) shows the EELS probability maps computed at three different energies (1.5, 2 and 2.4 eV). As can be noticed, regions separated by few nanometers can have drastically different optical responses. Furthermore, as observed by (Bosman *et al* 2011), higher energy modes (2.4 eV) appear confined in smaller regions than lower energy modes (1.5 and 2 eV).

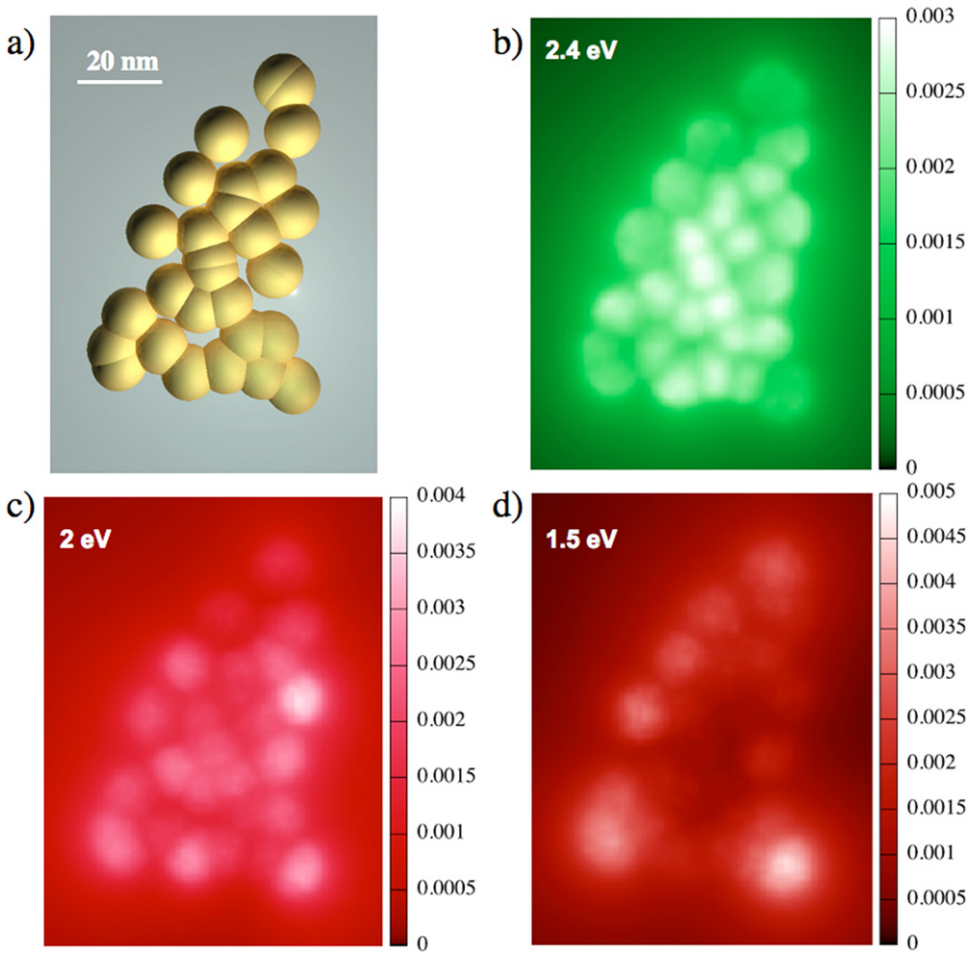

Figure 4. (a) Randomly generated nanostructure composed of 29 gold spheres (diameter $D = 9$ nm). (b) EELS probability maps for a 200 kV electron incident computed at different energies. The substrate is glass ($\varepsilon_{sub} = 2.25$).

5. Conclusion

To summarize, we have presented a numerical framework that allows us to simulate, from a generalized propagator, the electron energy losses and CL caused by the interaction of a fast electron and a metallic nanostructure. This formalism accounts for both penetrating and non-penetrating trajectories, and nanostructures of arbitrary morphologies, and rigorously takes into account the environment. Its numerical implementation is fast and does not rely on numerical libraries. An extension of this approach would be adequate for the computation of the optical forces exerted on metallic nanoparticles or to more complex experiments such as electron energy gain spectroscopy experiments (García de Abajo and Kociak 2008b, Yurtsever *et al* 2012, Talebi *et al* 2013, Park and Zewail 2014).

Acknowledgements

The authors acknowledge financial support from the European Union under the Seventh Framework Programme under a contract for an Integrated Infrastructure Initiative (Reference 312483 - *ESTEEM2*) and Agence Nationale de la Recherche (ANR, grant *HYNNA* ANR-10-BLAN-1016). This work was supported by the computing facility center CALMIP of the University Paul Sabatier of Toulouse (France). The authors thank N Renon for sharing his expertise in high-performance computing.

Appendix. Influence of a substrate on the electric field associated with a fast electron

We consider an electron traveling in a medium of dielectric constant ε_2 with a velocity $\mathbf{v} = -v\mathbf{e_z}$ ($v > 0$) towards a substrate located in the $z < 0$ region and characterized by a dielectric constant ε_1 (see figure 1). When the fast electron crosses the interface between two media, expression 1 must be modified to take into account the influence of the charge distribution induced on the interface by the moving charge. It is possible to take into account these corrections by writing the electric field in medium i as the sum of the electric field of the electron in an infinite bulk medium of dielectric constant ε_i, $\mathbf{E}_{\mathrm{el},i}(\mathbf{r}, \omega)$ and the contribution from the surface $\mathbf{E}_{\mathrm{surf},i}(\mathbf{r}, \omega)$:

$$\mathbf{E}_i(\mathbf{r}, \omega) = \mathbf{E}_{\mathrm{el},i}(\mathbf{r}, \omega) + \mathbf{E}_{\mathrm{surf},i}(\mathbf{r}, \omega) \tag{A.1}$$

The electron electric field in an infinite medium of dielectric constant ε_1 can be written as a superposition of plane waves with transverse magnetic polarization:

$$\mathbf{E}_{\mathrm{el},i}(\mathbf{r}, \omega) = \frac{i\,e}{2\pi^2 v} \mathrm{e}^{-\mathrm{i}\frac{\omega z}{v}} \iint \mathrm{d}q_x \mathrm{d}q_y \frac{\frac{\mathbf{q}}{\varepsilon_i} + k_0 \frac{v}{c}\mathbf{e}_z}{q^2 - k_0^2 \varepsilon_i} \mathrm{e}^{-\mathrm{i}\mathbf{q}_{//}.\mathbf{R}}. \tag{A.2}$$

From the continuity of the parallel components of both $\mathbf{E}$ and $\mathbf{B}$, it is possible to give the following expressions for the contribution from the surface $\mathbf{E}_{\mathrm{surf},\mathbf{2}}(\mathbf{r}, \omega)$ in the upper medium ($z > 0$):

$$\begin{aligned}
\mathbf{E}_{\mathrm{surf},2,\mathrm{x}}(\mathbf{r}, \omega) &= -\frac{i\,e}{2\pi^2 v k_0 \varepsilon_2} \int_0^{+\infty} \mathrm{d}q_{//} \mathrm{e}^{+\mathrm{i}q_{z,2}z} A_2(q) q_{z,2}\; q_{//}^2 2\pi \mathrm{i}\; J_1(q_{//}.\,R) \frac{x}{R} \\
\mathbf{E}_{\mathrm{surf},2,\mathrm{y}}(\mathbf{r}, \omega) &= -\frac{i\,e}{2\pi^2 v k_0 \varepsilon_2} \int_0^{+\infty} \mathrm{d}q_{//} \mathrm{e}^{+\mathrm{i}q_{z,2}z} A_2(q) q_{z,2}\; q_{//}^2 2\pi \mathrm{i}\; J_1(q_{//}.\,R) \frac{y}{R} \\
\mathbf{E}_{\mathrm{surf},2,\mathrm{z}}(\mathbf{r}, \omega) &= -\frac{i\,e}{2\pi^2 v k_0 \varepsilon_2} \int_0^{+\infty} \mathrm{d}q_{//} \mathrm{e}^{+\mathrm{i}q_{z,2}z} A_2(q)\; q_{//}^3 2\pi J_0(q_{//}.\,R)
\end{aligned} \tag{A.3}$$

In the latter expressions, $q_{z,i} = -\sqrt{\varepsilon_i k_0^2 - q_{//}^2}$, J_n are Bessel functions of the first kind of order n and:

$$A_2(q) = \frac{1}{\varepsilon_2 q_{z,1} + \varepsilon_1 q_{z,2}} \left[\frac{\varepsilon_1 k_0 + \varepsilon_2 q_{z,1}\beta}{q^2 - \varepsilon_2 k_0^2} - \frac{\varepsilon_2 k_0 + \varepsilon_2 q_{z,1}\beta}{q^2 - \varepsilon_1 k_0^2} \right] \tag{A.4}$$

Similarly, the contribution from the surface to the electric field in the lower medium can be written:

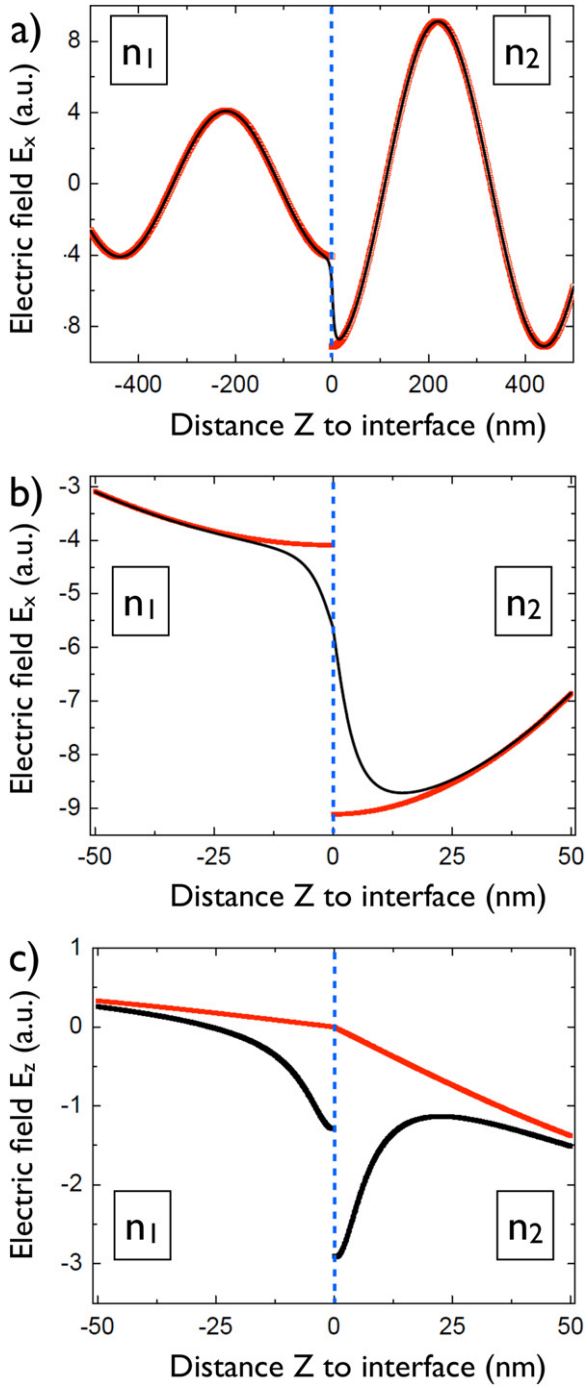

Figure A1. (a) *X*-component of the electric field associated with a 100 keV electron incident perpendicularly on a vacuum (n_2)/SiO_2(n_1) interface calculated at 10 nm from the electron trajectory. (b) Same in a small region around the interface. (c) *Z*-component of the electric field associated with a 100 keV electron incident on vacuum (n_2)/SiO_2(n_1) interface.

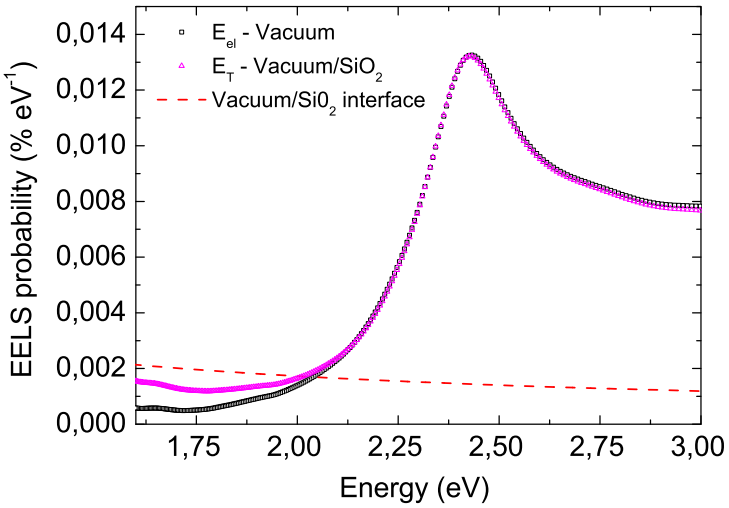

Figure A2. (Black squares) Electron energy losses of a 100 kV electron incident 12 nm away from a gold nanosphere (D = 10 nm) in vacuum computed with the bulk expression $\mathbf{E}_{\mathrm{el},i}(\boldsymbol{r}, \omega)$. (Pink triangles) Same when the gold nanosphere is deposited on a vacuum/SiO_2 interface computed with the total electric field $\mathbf{E}_i(\boldsymbol{r}, \omega)$. (Red dashed line) Electron energy losses experienced by a 100 kV electron incident on a bare vacuum/SiO_2interface (data from (García de Abajo 2010)).

$$\mathbf{E}_{\mathrm{surf},\mathbf{1},\mathbf{x}}(\mathbf{r}, \omega) = \frac{i\,e}{2\pi^2 v k_0 \varepsilon_1} \int_0^{+\infty} \mathrm{d}q_{//} \mathrm{e}^{-\mathrm{i}q_{z,1}z} A_1(q) q_{z,1}\; q_{//}^2 2\pi \mathrm{i}\; J_1(q_{//}.\,R) \frac{x}{R}$$

$$\mathbf{E}_{\mathrm{surf},\mathbf{1},\mathbf{y}}(\mathbf{r}, \omega) = \frac{i\,e}{2\pi^2 v k_0 \varepsilon_1} \int_0^{+\infty} \mathrm{d}q_{//} \mathrm{e}^{-\mathrm{i}q_{z,1}z} A_1(q) q_{z,1}\; q_{//}^2 2\pi \mathrm{i}\; J_1(q_{//}.\,R) \frac{y}{R}$$

$$\mathbf{E}_{\mathrm{surf},\mathbf{1},\mathbf{z}}(\mathbf{r}, \omega) = -\frac{i\,e}{2\pi^2 v k_0 \varepsilon_1} \int_0^{+\infty} \mathrm{d}q_{//} \mathrm{e}^{-\mathrm{i}q_{z,1}z} A_1(q)\; q_{//}^3 2\pi J_0(q_{//}.\,R) \qquad \text{(A.5)}$$

With

$$A_1(q) = \frac{1}{\varepsilon_2 q_{z,1} + \varepsilon_1 q_{z,2}} \left[\frac{\varepsilon_1 k_0 - \varepsilon_1 q_{z,2} \beta}{q^2 - \varepsilon_2 k_0^2} - \frac{\varepsilon_2 k_0 - \varepsilon_1 q_{z,2} \beta}{q^2 - \varepsilon_1 k_0^2} \right] \qquad \text{(A.6)}$$

In figure A1, we have computed the components along (OX) and (OZ) of both the total electric field $\mathbf{E}_i(\mathbf{r}, \omega)$ and the electric field in the bulk $\mathbf{E}_{\mathrm{el},i}(\mathbf{r}, \omega)$ in the two media above and below the interface. Figures A1(a) and (b) show that taking into account the contribution from the surface $\mathbf{E}_{\mathrm{surf},i}(\mathbf{r}, \omega)$ allows us to recover the continuity of the parallel electric field component. These results show that the influence of the interface contribution is weak outside of an ≈50 nm thick layer around the interface. It is furthermore possible to show that the relative importance of the corrections induced by the presence of the substrate is dependent upon the energy, as the low frequency Fourier components of the electric field are more strongly affected away from the interface.

To go further, we have computed the electron energy losses using the method proposed above, taking into account either the bulk expression $\mathbf{E}_{\mathrm{el},i}(\mathbf{r}, \omega)$ for the electric field associated with the moving charge, or the corrected expression $\mathbf{E}_i(\mathbf{r}, \omega)$.

These results of figure A2 show that the substrate-induced corrections to the incident E-field have a weak influence on the energy losses. This can be explained by the fact that the larger modification of the incident electric field induced by the interface contribution $\mathbf{E}_{\mathrm{surf},i}(\mathbf{r}, \omega)$ is on the *Z*-component. On the contrary, along its trajectory, the electron probes the electric field radiated along the *Z*-component, which is radiated by dipoles oriented in-plane and is therefore not excited efficiently by the out-of-plane components of the electron electric field. Moreover, the nanosphere is only deposited on the vacuum/SiO_2 interface, and therefore its dielectric environment is mainly vacuum, which explains that no observable redshift is evidenced.

References

Alber I, Sigle W, Demming-Janssen F, Neumann R, Trautmann C, van Aken P A and Toimil-Molares M E 2012 *ACS Nano* **6** 9711

Baffou G, Girard C and Quidant R 2010 *Phys. Rev. Lett.* **104** 136805

Bosman M, Anstis G R, Keast V J, Clarke J D and Cortie M B 2011 *ACS Nano* **6** 319

Bosman M, Ye E, Tan S F, Nijhuis C A, Yang J K W, Marty R, Mlayah A, Arbouet A, Girard C and Han M-Y 2013 *Sci. Rep.* **3** 1312

Boudarham G and Kociak M 2012 *Phys. Rev.* B **85** 245447

Carbone F, Barwick B, Kwon O H, Park H S, Baskin J S and Zewail A H 2009 *Chem. Phys. Lett.* **468** 107

Coenen T, Vesseur E J R and Polman A 2012 *ACS Nano* **6** 1742

Dorfmüller J, Vogelgesang R, Khunsin W, Rockstuhl C, Etrich C and Kern K 2010 *Nano Lett.* **10** 3596

Fujimoto F, Komaki K-i and Ishida K 1967 *J. Phys. Soc. Jpn.* **23** 1186

García de Abajo F J and Kociak M 2008a *Phys. Rev. Lett.* **100** 106804

García de Abajo F J and Kociak M 2008b *New J. Phys.* **10** 073035

García de Abajo F J 2010 *Rev. Mod. Phys.* **82** 209

García de Abajo F J and Howie A 2002 *Phys. Rev.* B **65** 115418

Geuquet N and Henrard L 2010 *Ultramicroscopy* **110** 1075

Girard C and Dereux A 1996 *Rep. Prog. Phys.* **59** 657

Girard C 2005 *Rep. Prog. Phys.* **68** 1883

Gómez-Medina R, Yamamoto N, Nakano M and de Abajo F J G 2008 *New J. Phys.* **10** 105009

Gu L, Sigle W, Koch C T, Ögüt B, van Aken P A, Talebi N, Vogelgesang R, Mu J, Wen X and Mao J 2011 *Phys. Rev.* B **83** 195433

Hohenester U and Trügler A 2012 *Computer Physics Communications* **183** 370

Hohenester U, Ditlbacher H and Krenn J R 2009 *Phys. Rev. Lett.* **103** 106801

Hörl A, Trügler A and Hohenester U 2013 *Phys. Rev. Lett.* **111** 076801

Howie A 2009 *Microscopy and Microanalysis* **15** 314

Jackson J 1998 *Classical Electrodynamics* 3rd edn (New York: Wiley)

Kuttge M, Vesseur E J R, Koenderink A F, Lezec H J, Atwater H A, García de Abajo F J and Polman A 2009 *Phys. Rev.* B **79** 113405

Losquin A, Camelio S, Rossouw D, Besbes M, Pailloux F, Babonneau D, Botton G A, Greffet J-J, Stéphan O and Kociak M 2013 *Phys. Rev.* B **88** 115427

Major T A, Devadas M S, Lo S S and Hartland G V 2013 *J. Phys. Chem.* C **117** 1447

Martin O J F, Girard C and Dereux A 1995 *Phys. Rev. Lett.* **74** 526

Marty R, Baffou G, Arbouet A, Girard C and Quidant R 2010 *Opt. Expr.* **18** 3035

Myroshnychenko V *et al* 2012 *Nano Lett.* **12** 4172

Nelayah J, Kociak M, Stephan O, Garcia de Abajo F J, Tence M, Henrard L, Taverna D, Pastoriza-Santos I, Liz-Marzan L M and Colliex C 2007 *Nat. Phys.* **3** 348

Nicoletti O, de la Pena F, Leary R K, Holland D J, Ducati C and Midgley P A 2013 *Nature* **502** 80
Novotny L 1997 *J. Opt. Soc. Am.* A **14** 105
Park S T and Zewail A H 2014 *Phys. Rev.* A **89** 013851
Powell C J and Swan J B 1959 *Phys. Rev.* **115** 869
Rivacoba A and Zabala N 2014 *New J. Phys.* **16** 073048
Scholl J A, Koh A L and Dionne J A 2012 *Nature* **483** 421
Sigle W, Nelayah J, Koch C T and van Aken P A 2009 *Opt. Lett.* **34** 2150
Talebi N, Sigle W, Vogelgesang R and van Aken New P 2013 *J. Phys.* **15** 053013
Teulle A, Marty R, Viarbitskaya S, Arbouet A, Dujardin E, Girard C and Colas des Francs G 2012 *J. Opt. Soc. Am.* B **29** 2431
Tizei L H G and Kociak M 2013 *Phys. Rev. Lett.* **110** 153604
Tripathy S, Marty R, Lin V K, Teo S L, Ye E, Arbouet A, Saviot L, Girard C, Han M Y and Mlayah A 2011 *Nano Lett.* **11** 431–7
Verellen N, López-Tejeira F, Paniagua-Domnguez R, Vercruysse D, Denkova D, Lagae L, van Dorpe P, Moshchalkov V V and Sánchez-Gil J A 2014 *Nano Lett.* **14** 2322
Vesseur E J R, de Waele R, Kuttge M and Polman A 2007 *Nano Lett.* **7** 2843
Viarbitskaya S, Teulle A, Marty R, Sharma J, Girard C, Arbouet A and Dujardin E 2013 *Nat. Mater.* **12** 426
Yurtsever A, van der Veen R M and Zewail A H 2012 *Science* **335** 59
Zagonel L F *et al* 2010 *Nano Lett.* **11** 568